Research Article

optica

How to make the propagation time through an optical fiber fully insensitive to temperature variations

ERIC NUMKAM FOKOUA,[1,*] MARCO N. PETROVICH,[1] TOM BRADLEY,[1] FRANCESCO POLETTI,[1] DAVID J. RICHARDSON, [1] RADAN SLAVÍK,[1]

[1] *Optoelectronics Research Centre, University of Southampton, Southampton, SO17 1BJ, United Kingdom*
**Corresponding author: Eric.Numkam-Fokoua@soton.ac.uk*

Received XX Month XXXX; revised XX Month, XXXX; accepted XX Month XXXX; posted XX Month XXXX (Doc. ID XXXXX); published XX Month XXXX

Propagation time through standard (solid core) optical fibers changes with temperature at a rate of 40 ps/km/K. The thermo-optic effect in silica glass accounts for about 95% of this change and thus hollow core fibers, in which the majority of optical power propagates through an air rather than glass core, can have this sensitivity greatly reduced. To date we have demonstrated a sensitivity as low as 2 ps/km/K, this value being limited by thermally-induced fiber elongation. In this paper, we predict and experimentally demonstrate that the thermal sensitivity of propagation time can be reduced to zero (or even made negative) in Hollow Core Photonic Bandgap Fibers (HC-PBGF) by compensating the thermally-induced fiber elongation with an equal and opposite thermally-induced group velocity change (i.e. by making the light travel faster through the elongated fiber). This represents the ultimate fiber solution for many propagation time sensitive applications.

OCIS codes: *(060.2280) Fiber design and fabrication; (060.2400) Fiber properties; (060.5295) Photonic crystal fibers; (120.3930) Metrological instrumentation; (280.4788) Optical sensing and sensors.*

http://dx.doi.org/10.1364/OPTICA.99.099999

1. INTRODUCTION

The primary application spaces of single-mode fiber have traditionally been telecommunications and sensing. However, due to their many unique properties, optical fibers continue to penetrate into new research areas and keep attracting interest from novel and diverse fields of science and engineering. Examples include fiber lasers and more recently also precise time [1] and frequency transfer and dissemination [2] over optical fibers and optical networks.

Propagation time through an optical fiber varies due to environmental changes (temperature, vibrations, etc.), which is undesirable in a host of applications such as precise time and frequency transfer, or applications requiring highly accurate time synchronization of (data) signals. Further such applications are anticipated in the (near) future given for example the demanding timing requirements of autonomous manufacturing (e.g., synchronization of robots working together) and future 5G networks [3].

Examples of scientific systems in which very precise timing signals need to be disseminated for synchronization purposes include large experimental infrastructures such as synchrotrons (e.g., FLASH at DESY, Hamburg [1]), linear particle accelerators, large telescope arrays, and phase arrayed antennae. A specific example of where precise frequency transfer is needed concerns comparison of optical clocks in various national metrology laboratories (e.g., between Germany and France [4]) at a required precision (fractional stability) at/below the $5x10^{-17}$ level, and which can currently only be achieved using optical fiber networks. However, such a level of precision is easily compromised by thermally-induced changes in optical path length (temperature drift) with time that unavoidably result in a Doppler frequency shift [2,4]. In these systems, active stabilization of the optical path length is required and achieved using bi-directional propagation of the same signal in the same fiber. However, the quality of stabilization is impaired due to processes such as Rayleigh scattering that can cause interference between forward and backward propagating signals. Additionally, in some parts of the system (e.g., at the transmitter/receiver ends), the signals unavoidably only propagate uni-directionally and these parts of the system must be temperature stabilized to unprecedented levels that are realistically only achievable in a (metrology) laboratory environment. However, to enable applications that require precise time/frequency distribution in the field (e.g., relativistic geodesy [5]), use of these system outside of a well-stabilized laboratory environment is necessary.

Another example of an area in which a lower thermal sensitivity of the fiber propagation time may be essential is in ultralow-frequency noise stabilization of lasers to an optical fiber delay line [6]. Here a lower thermal sensitivity may allow for significant improvements in the achievable laser linewidth, enabling precise, compact, field-deployable optical oscillators (e.g., to be put on satellites for next-generation Global Positioning Systems). Another device example is the ultra-low noise opto-electronic oscillator in which a long delay line (made using km-length optical fibers) is used [7]. It is also perhaps worth mentioning the fundamental thermal noise limit in fiber lasers [8] that again could be reduced by utilizing lower thermal sensitivity fibers.

To avoid the undesirable thermal sensitivity of propagation time through optical fibers, specialty coatings have been developed that counteract the thermally-induced fiber elongation and refractive index changes [9]. The very best coated fibers are able to reduce the propagation time thermal sensitivity from ~40 ps/km/K of telecom-standard SMF-28 down to 3.7 ps/km/K [9], representing up to an order of magnitude reduction. Such fibers are now commercially available (e.g. the 'Phased-Stabilized Optical Fiber Cable' from

Furukawa Japan and the STFOC Optical Cable from Linden Photonics, U.S.A). Although this level of reduction is useful for many applications, further reduction in temperature sensitivity is still highly desirable. Additionally, this level of reduction is only achieved over quite a limited (e.g., 0 - 40°C) temperature range [9].

It has been shown recently [10] that Hollow-Core Photonic Bandgap Fibers (HC-PBGFs) made from silica and without any specialty coating can perform even better than specialty-coated standard fibers. In these fibers, the light is guided predominantly in the air-filled core, minimizing the impact of the thermo-optic effect in silica. As the thermo-optic effect in silica is responsible for about 95% of the thermal sensitivity in conventional solid-core fiber, HC-PBGF can have a significantly lower thermal sensitivity than solid-core fibers. This was demonstrated experimentally with a HC-PBGF propagation time thermal sensitivity as small as 2 ps/km/K measured without the use of any specialty coating [10]. This represents the smallest thermal sensitivity so far reported.

This low thermal sensitivity is complemented by the other unique set of HC-PBGF properties that primarily originate from the fact that most of the power propagates in an air rather than a solid silica glass core. These include: ultra-low nonlinearity (of interest, for example, for the delivery of high-peak power pulses [11]); close to vacuum light speed propagation (of interest, for example, for low latency data transmission [12]); and a strong resistance to radiation damage [13].

Although the reduction in thermal sensitivity of optical fibers reported so far is significant (almost 20 times as compared to standard SMF-28), the ultimate solution to current and new applications would be to develop an optical fiber with zero thermal sensitivity. This could potentially bring orders-of-magnitude improvement to systems that are using standard fibers today, eventually allowing for new applications for which the current level of thermal sensitivity is still too high.

Here we propose and show that the already low thermal sensitivity of HC-PBGF can actually be reduced to zero (and even made negative) through suitable fiber design. In addition to providing a detailed description of such designs, we also derive closed-form expressions that allow for a good understanding of the underlying physics and for a precise quantitative analysis without the need to perform many time-consuming finite-element calculations. We also include a brief discussion/analysis of the influence of the fiber's protective coating, again emphasizing the underlying physics as well as deriving a closed-form formula. Subsequently, we carry out an experimental demonstration confirming our predictions and showing zero sensitivity of propagation time through an optical fiber for the very first time.

2. PRINCIPLE

For the sake of simplicity, we consider in our analysis a central operating wavelength in the *1.55 μm* band. There are straightforward scaling rules to shift it to other wavelengths available in the literature [14,15].

A. Physical insight

The underlying physical principle can be understood through a simple analysis of the processes contributing to the thermal change in propagation delay. The transit time for signal propagation through an optical fiber of length L is:

$$\tau = \frac{n_g L}{c}, \tag{1}$$

where L is the fiber length, n_g the group index of the propagating mode and c is the speed of light in vacuum. The change in transit time with temperature normalized to the fiber length (**Thermal Coefficient of Delay, TCD**) is then expressed as:

$$TCD = \frac{1}{L}\frac{d\tau}{dT} = \frac{1}{c}\left(n_g \frac{1}{L}\frac{dL}{dT} + \frac{dn_g}{dT}\right) = \frac{1}{c}\left(\varepsilon_{zz} n_g + \frac{dn_g}{dT}\right), \tag{2}$$

where

$$\varepsilon_{zz} = \frac{1}{L}\frac{dL}{dT} \tag{3}$$

is the longitudinal coefficient of thermal expansion. In the absence of a protective fiber coating, this reduces to the linear isotropic thermal expansion coefficient ($\alpha = 5.5 \times 10^{-7} K^{-1}$ for fused silica glass [16]). To obtain zero thermal sensitivity ($TDC = 0$) we thus need (Eq. 2):

$$\frac{1}{n_g}\frac{dn_g}{dT} = -\varepsilon_{zz}. \tag{4}$$

In conventional optical fibers, the glass through which the guided mode propagates sees its refractive index increase with temperature due to the thermo-optic effect. Consequently, n_g also increases with temperature. Thus, the condition (Eq. 4) can only be met when a specialty coating that causes fiber contraction in the longitudinal direction as temperature increases is used (changing the sign of ε_{zz}) [9]. Here, however, we propose to achieve zero thermal sensitivity (Eq. 4) in fibers with standard coating materials for which ε_{zz} is positive, by instead compensating the fiber elongation by a reduction in the mode group index n_g (i.e. by making light travel faster as the temperature increases, and thus obtaining $dn_g/dT < 0$). Whilst this is not possible in solid-core fibers, it can be achieved in HC-PBGFs, as outlined in Fig. 1. As we describe in detail below, a temperature increase raises the refractive index of the glass and increases the pitch in the HC-PBGF cladding through thermal expansion, resulting in a small red-shift in the position of the center wavelength of the photonic bandgap (Fig. 1b). Due to the typical spectral characteristics of n_g in HC-PBGF across the bandgap (sketched in Fig. 1b), the thermally-induced bandgap wavelength shift produces $dn_g/dT > 0$ near the short-wavelength edge of the bandgap and $dn_g/dT < 0$ (required to satisfy Eq. 4) near the long-wavelength edge of the bandgap. These changes become larger as we approach the bandgap edges, Fig. 1b. From a physical point of view, these changes result from very small modifications in the fraction of power guided in the solid glass material. It emerges therefore that within the long wavelength part of the bandgap (where $dn_g/dT < 0$) the fiber elongation resulting from thermal expansion can be compensated in part, fully, or even overcompensated by an appropriate choice of the wavelength of operation.

The change in, dn_g/dT in HC-PBGFs can be further qualitatively understood through the following analysis. Firstly, the scaling laws of the photonic bandgap [14,15] allow an estimation of the bandgap shift with temperature, which is sketched in Fig. 1b. Ignoring material dispersion in this qualitative analysis, for small changes in dimensions or material properties (refractive index), the position of the photonic bandgap changes in such a way that the quantity

$$k\Lambda\left(n_{glass}^2 - n_{air}^2\right)^{1/2} \tag{5}$$

remains invariant, with $k = 2\pi/\lambda$ being the free space wave number. Assuming that the refractive index of air is $n_{air} = 1$ and that it changes negligibly with temperature, it follows by differentiating the quantity in Eq. 5 and equating this to zero, that for a thermal change ΔT, the center wavelength λ_0 of the photonic bandgap will shift by $\Delta\lambda$ given by:

$$\frac{1}{\lambda_0}\frac{\Delta\lambda}{\Delta T} = \frac{1}{\Lambda}\frac{\Delta\Lambda}{\Delta T} + \frac{n_{glass}}{n_{glass}^2 - 1}\frac{\Delta n}{\Delta T}. \tag{6}$$

In a fiber without coating, the thermal expansion is isotropic and linear, and the first term on the equation right hand side reduces to the thermal coefficient of expansion for silica $\alpha = 5.5 \times 10^{-7}\varepsilon/K$ [16]. The second term has contributions from the thermo-optic effect ($\partial n/\partial T = 11.4 \times 10^{-6}$ near $1.55\ \mu m$ [16]) and the photo-elastic effect, which because of the isotropic expansion, induces an index change $\Delta n/\Delta T = -\left(n_{glass}^3/2\right)(p_{11} + 2p_{12})\alpha$ where p_{11} and p_{12}

are Pockel's coefficients for silica. It follows that for a photonic bandgap centered around $\lambda_0 = 1.55\ \mu m$, Eq. 6 evaluates to:

$$\frac{\Delta\lambda}{\Delta T} = 23.2\ pm/K. \tag{7}$$

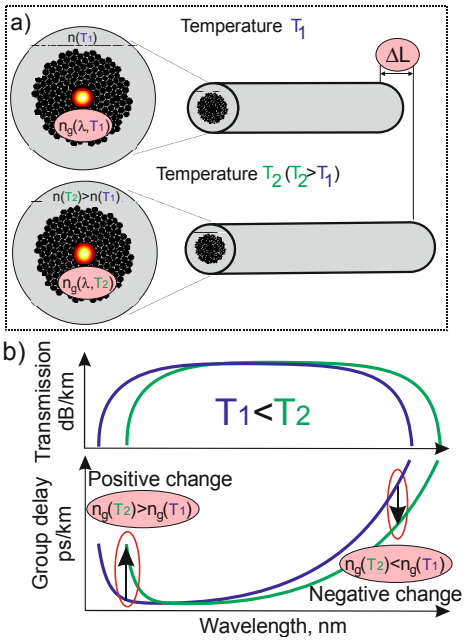

Fig. 1. The principle of our compensation method. (a) A temperature increase makes the HC-PBGF longer by ΔL. Simultaneously, the glass refractive index and the fiber cross-section dimensions increase, modifying n_g. We target conditions for which n_g decreases with temperature (making the light travel faster), compensating for the fiber elongation. (b) Sketch of typical transmission and n_g characteristics of a HC-PBGF at two temperatures. Increasing the temperature shifts the bandgap position to longer wavelengths (Eq. 7), resulting in $dn_g/dT > 0$ at shorter wavelengths and $dn_g/dT < 0$ at longer wavelengths. The magnitude of this change is given by the gradient of the group delay, i.e., the chromatic dispersion. At a specific wavelength, the decrease in n_g exactly compensates for the fiber elongation.

Remarkably, this value depends solely on the thermal properties of silica and is independent of the HC-PBGF geometry. Assuming that all fiber properties are simply red-shifted with the bandgap as the temperature increases, we can calculate dn_g/dT as follows:

$$\frac{dn_g}{dT} = -\frac{dn_g}{d\lambda}\frac{\Delta\lambda}{\Delta T} = -cD\frac{\Delta\lambda}{\Delta T}, \tag{8}$$

where D is the chromatic dispersion (in s/m^2). Eq. 2 can then be re-written as:

$$TCD = \alpha\frac{n_g}{c} - D\frac{\Delta\lambda}{\Delta T}. \tag{9}$$

Although this expression, as we will show later, is too approximate to allow for precise quantitative analysis, it provides us with valuable insight. It states that tailoring the *TCD* in HC-PBGFs is akin to engineering the fiber's chromatic dispersion D. With the shift calculated in Eq. 7 and the approximation $n_g \approx 1$, Eq. 9 states that $TCD = 0$ will be obtained when the dispersion $D = 79\ ps \cdot nm^{-1} \cdot km^{-1}$. This value can in principle be achieved in any HC-PBGF as its typical dispersion (first derivative of group delay as sketched in Fig. 1b) varies from very large and negative values at the blue edge of the photonic bandgap, to very large and positive values near the red edge. It is worth mentioning that another situation in which the desired value of D can be achieved is when the fiber supports so-called surface modes. These are modes localized at the core boundary. Near avoided crossings of the fundamental mode and such surface modes the dispersion can also take large negative or positive values. It is therefore also possible to achieve this value of D near a surface mode. [17].

B. Quantitative analysis: uncoated fibers

Although the simplified analysis ('zero order approximation') described above allows an understanding of the physics behind our approach, it is not precise enough to be used for quantitative analysis. In this sub-section, we derive a more accurate expression for the *TCD* by analyzing the first order correction to the mode propagation constant.

When temperature is changed, there are three effects that contribute to the change in n_g as described earlier. First, the thermal expansion slightly changes the HC-PBGF waveguide cross-sectional dimensions. The coordinates of the perturbed fiber geometry upon transverse thermal expansion are related to those of the unperturbed fiber by $x' = x(1 + \alpha\Delta T)$ and $y' = y(1 + \alpha\Delta T)$. The other two effects, the photo-elastic and thermo-optic effects, both jointly contribute to a slight change in the glass refractive index, Δn. The correction to the propagation constant of a guided mode as a result of the small perturbation arising from the transverse thermal expansion is given by [18]:

$$\Delta\beta_{exp} = \alpha\Delta T\left(\omega\frac{\partial\beta}{\partial\omega} - \beta\right), \tag{10}$$

where ω is the angular frequency of the propagating light wave. The correction to the propagation constant arising from small changes in the waveguide refractive index profile is a well-studied problem. From references [19, 20], the first order correction is given by:

$$\Delta\beta_n = \frac{\iint E^*\Delta\varepsilon(x,y)k_0^2 E dxdy}{2\beta\iint E^* E dxdy}, \tag{11}$$

where $\varepsilon = n^2$ is material permittivity and E the electric field distribution of the guided mode. In what follows, we consider the refractive index of glass to change with temperature, while neglecting the temperature dependence of the refractive index of air (see Appendix 1). Doing so means that the integral in the numerator of Eq. 11 vanishes everywhere except in glass. Furthermore, since the thermal expansion is everywhere isotropic, $\Delta\varepsilon = 2n\Delta n$ is independent of the position. If we denote by $\eta(\lambda)$ the wavelength dependent fraction of $|E|^2$ carried in the glass material, we can rewrite Eq. 11 as:

$$\Delta\beta_n = \frac{k_0^2}{\beta}n_{glass}\frac{\Delta n}{\Delta T}\eta(\lambda)\Delta T, \tag{12}$$

where $\Delta n/\Delta T$ is the total refractive index change from the thermo-optic and photo-elastic effects. Upon a temperature change ΔT, the mode therefore has a new propagation constant $\beta' = \beta + \Delta\beta_{exp} + \Delta\beta_n$ and travels the distance $L' = L + \alpha L\Delta T$. Ignoring the second order quantities $(\Delta\beta\Delta L)$, one obtains (after simple algebraic manipulation):

$$TCD = \alpha\frac{\partial\beta}{\partial\omega} - \alpha\lambda D + \frac{\partial}{\partial\omega}\left(\frac{\Delta n}{\Delta T}\frac{k_0^2}{\beta}n_{glass}\eta(\lambda)\right). \tag{13}$$

The first term in Eq. 13 comes from the elongation, the second from the transverse expansion and the third from the thermo-optic and photo-elastic effects. Although Eq. 13 does not give as straightforward/simplistic insight as to how to achieve $TDC = 0$ as Eq. 9, it provides a very accurate prediction of the *TCD* as we will show later. This eliminates the need for very time-consuming finite element simulations for various fiber structures and their parameters, all calculated at several temperatures, which would otherwise all be required to optimize the fiber design.

C. Expression allowing for quantitative analysis: coated fibers

The above analysis focused on bare fibers which do not have a protective coating. However, optical fibers are usually protected by a polymer coating layer that improves its mechanical properties and facilitates handling. Such a polymer coating is often softer (smaller Young's modulus) than glass, but generally has a larger coefficient of thermal expansion. The presence of the mechanically-coupled coating modifies the thermal expansion of the fiber structure in a complex way. To analyze this it is necessary to calculate the thermally-induced change to the fiber structure first. This can be done by solving stress-equilibrium equations in each layer of the fiber (see Fig. 2) and using Hooke's law to obtain the strain distributions and displacements [21]. The radial displacements from this procedure take the form $u_r = A/r + Br$ where A and B are constants for each layer. Further, the elongation of the fiber is well approximated by the area-weighted average of the product of the Young's modulus and thermal expansion coefficients across all the layers [9,21]. With the displacement and strains obtained, the thermal response of the fiber can be found by performing finite element simulations on the perturbed fiber at different temperatures, or through a full but complex perturbation analysis by transforming the fiber coordinates [22].

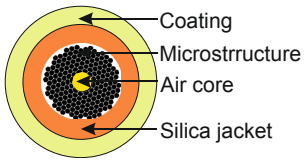

Fig. 2 The structure used to model thermal effects in a realistic fiber comprising a finite-thickness silica jacket and a coating layer.

The analysis that lead to Eqs. 10, 11 suggests that the fiber's thermal response is predominantly dictated by changes that happen in the regions of the cross-section that carry significant mode field intensity $|E|^2$. This assumption can significantly simplify the TCD calculation by allowing replacement of the longitudinal expansion in Eq. 13 by the strain component ε_{zz} and the transverse expansion and index changes by their $|E|^2$-weighted averages across the fiber cross section. Subsequently, we can write the TCD in a coated fiber as:

$$TCD = \varepsilon_{zz}\frac{\partial\beta}{\partial\omega} - \bar{\alpha}\lambda D + \frac{\partial}{\partial\omega}\left(\overline{\left(\frac{\Delta n}{\Delta T}\right)}\frac{k_0^2}{\beta}n_{glass}\eta(\lambda)\right), \quad \textbf{(14)}$$

where $\bar{\alpha}$ is the $|E|^2$ weighted average coefficient of expansion in the transverse direction ($|E|^2$ weighted average of u_r/r) and $\overline{\left(\frac{\Delta n}{\Delta T}\right)}$ the $|E|^2$ weighted refractive index change with temperature). As pointed out in [21], the most relevant impact of the coating layer is the increase in the longitudinal expansion. Intuitively, since it will be typical for silica glass to be stiffer than the coating, a thicker solid silica jacket surrounding the hollow microstructure will offer effective resistance to the pull of the coating, which has a larger thermal expansion coefficient and will contribute to reduce ε_{zz}. This is shown through numerical examples in the next section.

D. Design considerations

In the discussion of Eq. 9 we mentioned that $TDC = 0$ is obtained for a dispersion $D = 79\ ps/nm\cdot km$ and which should be achievable in any HC-PBGF as its dispersion typically varies across the bandgap from large negative to large positive values [17]. However, it is desirable for fibers designed to have $TCD = 0$ to achieve this value at wavelengths where the transmission losses are as low as possible. Furthermore, as $TDC = 0$ occurs for a specific wavelength only it is also desirable for the fiber design to provide $TCD \approx 0$ over as large bandwidth as possible (i.e. necessitating as small a dispersion slope as possible according to Eq. 9). In our design, we quantify this by calculating/measuring the spectral bandwidth over which the elongation of an uncoated fiber is compensated by more than 90%. As mentioned earlier, this elongation is responsible for *TCD* of *2 ps/km/K*. Thus, we assume the interval over which $|TCD| \le 0.2\ ps/km/K$ as the effective bandwidth of thermal compensation of the fiber.

3. SIMULATIONS

The aim of this section is to show how the *TCD* properties can be tailored through an appropriate choice of the HC-PBGF structural parameters. We focus specifically on the impact of the core size and air-hole diameter to pitch ratio ($d/\Lambda = 1 - t/\Lambda$ with t the cladding strut thickness and Λ the cladding's pitch) to which we refer –improperly - as the 'air-filling fraction'. However, before going into the detailed analysis, we evaluate the accuracy of Eqs. 7, 9, 13, 14 by comparing the results obtained with these equations and that obtained with finite element numerical simulations, and analyze the magnitudes of various contributions to the *TCD*.

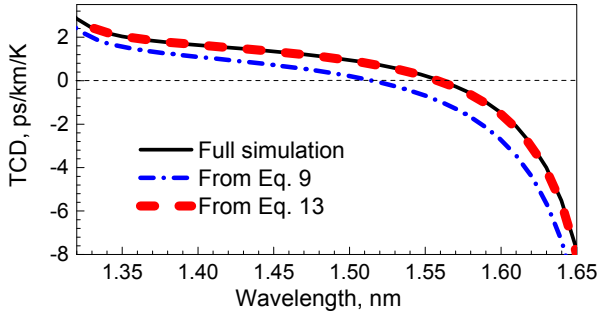

Fig. 3. Simulated thermal coefficient of delay in an uncoated 7-cell HC-PBGF using finite element simulation (black solid), Eq. 9 (blue dash-dot), and Eq. 13 (red dashed); air filling fraction is 0.975.

We evaluated the accuracy of Eqs. 7, 9 and 13 for the example of an uncoated 7-cell HC-PBGF. This is a fiber in which the central core defect is formed by removing 7 unit cells from an otherwise defect free lattice. First, we performed finite element simulations, calculating $n_g(\lambda)$ across the entire bandgap spectral range for 11 temperature settings of 0- 100°C in 10°C steps. The structure simulated at each temperature was obtained by scaling the original fiber cross-section by a factor of $1 + \alpha(T - T_0)$ with $T_0 = 25$°C being room temperature. Additionally, the glass refractive index was modified by Δn as calculated from the thermo-optic and photoelastic effects. The $TCD(\lambda)$ was then evaluated by a linear fit of $n_g(\lambda)$ obtained at these 11 temperature points. Simulations showed that the short/long wavelength edges of the bandgap shifted at the rate of 22.7and 25.3 pm/K, respectively. This is very close to the value given by Eq. 7 that predicted the center of the bandgap to move by 23.2 pm/K. The results of the $TCD(\lambda)$ are shown in Fig. 3. Also shown are the $TCD(\lambda)$ obtained from Eqs. 9 and 13 which were evaluated by calculating the dispersion and fraction of $|E|^2$ carried in glass as a function of wavelength at room temperature only. We see that Eq. 9 predicts well the trend of the $TCD(\lambda)$ but does not provide accurate results in terms of absolute values. The agreement between the simple expression of Eq. 13 and results from lengthy finite element simulations is almost perfect. For this fiber, $TCD = 0$ is achieved near a wavelength of 1.55 μm, and $|TCD| \le 0.2 ps/km/K$ is obtained over a bandwidth as broad as 16 nm. Examining the contributions from the various physical effects, which are shown in Fig. 4, one notes that the transverse expansion and photo-elastic effects are relatively small and in fact, almost cancel each other. The dominant two effects are then the thermo-optic effect and elongation due to the change in temperature. While elongation gives an almost wavelength-independent contribution to the *TCD*, the change in the refractive index of the fiber (thermo-optic effect) leads to a strongly wavelength-dependent *TCD*. As its value ranges from large positive values (at the blue-edge of the bandgap) to large negative values (at the red edge of

the bandgap), it allows for compensation of the effect of the elongation at a specific wavelength within the bandgap.

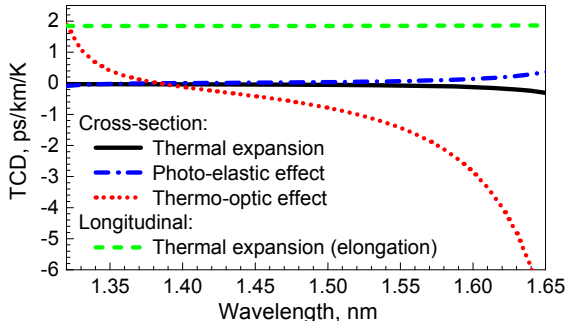

Fig. 4. Simulated contributions to the thermal coefficient of delay in an uncoated 7-cell HC-PBGF. These include the transverse (black, dot) and longitudinal (greed, dash) thermal expansion, photo-elastic effect (dash-dot, blue), and thermo-optic effect (red, dot). Air filling fraction is 0.975.

We repeated the finite element simulations in the presence of a $45\ \mu m$ thick coating with a Young's modulus of 0.5 GPa (while silica has 72.5 GPa) and a thermal expansion coefficient of $80 \times 10^{-6} \varepsilon/K$, as considered in the previous study by Dangui et al [21]. For the silica jacket (Fig. 2) thickness, we considered two values of $40\ \mu m$ and $70\ \mu m$. Besides finite element simulations, we also used Eq. 14 to estimate the TCD. All the results are shown in Fig. 5. As the coating expands at a higher rate than the silica, its predominant effect is a more substantial elongation of the fiber, shifting the *TCD* curve towards higher values, as confirmed by the results shown in Fig. 5. This implies that the wavelength at which $TCD = 0$ occurs is red-shifted towards the longer-edge of the bandgap, Fig. 5. We can also conclude (from Fig. 5) that a thicker silica jacket leads to smaller effect of the coating on the *TCD* curve. This is because the silica glass is significantly stiffer than the acrylate coating and thus the effect of the coating on the *TCD* can be reduced by increasing the thickness of the silica jacket. Finally, we see that Eq. 14 provides a remarkably accurate prediction for the *TCD* in a coated fiber.

Next, we investigated the extent to which the *TCD* can be altered by choosing the structural parameters of the HC-PBGF. Eq. 9 suggests the link between *TCD* and chromatic dispersion *D*, which is known to be strongly dependent on the core size and cladding air-filling fraction [17]. Fig. 6 shows the simulated *TCD* (from Eq. 13) for uncoated HC-PBGFs of similar cladding design but with core sizes formed by removing 3, 7, 19, and 37 unit cells at the center of the periodic structure. It can be seen that because fibers with large core defects (19, and 37 cells) have a much reduced fraction of $|E|^2$ carried in the glass throughout the photonic bandgap, their $TCD(\lambda)$ is dominated by elongation and remains nearly flat except near the edges of the photonic bandgap where $\eta(\lambda)$ changes rapidly. For 37c cell fiber, $TCD = 0$ occurs at the very edge of the bandgap only, where higher propagation loss than at the center of the bandgap is to be expected. Additionally, the *TCD* curve gets relatively steep there, resulting in a $|TCD| \leq 0.2\ ps/km/K$ bandwidth of *5 nm* only, Fig. 6. The other extreme to 37-cell, the 3-cell fiber with relatively large $\eta(\lambda)$ achieves $TDC = 0$ very close to the center of the bandgap, however, its $|TCD| \leq 0.2\ ps/km/K$ bandwidth is only 7 *nm*, as the *TCD* curve is relatively steep across the entire bandgap. Three cell fibers generally suffer from significantly higher loss that 7, 19, and 37-cell fibers (e.g., fiber designs shown in Fig. 6 have a minimum loss of 80, 20, 5, and 2 dB, for 3, 7, 19, and 37-cells, respectively), making them less attractive for applications [23]. 7-cell and 19-cell fibers look like the best choice with $|TCD| \leq 0.2\ ps/km/K$ bandwidths of *15 nm* (7-cell) and *10 nm* (19-cell). Generally, 19-cell fibers will have lower propagation losses than 7-cell fibers, suggesting that the optimum choice between a 7 and 19-cell core depends on the application (whether larger bandwidth or lower loss are of primary importance).

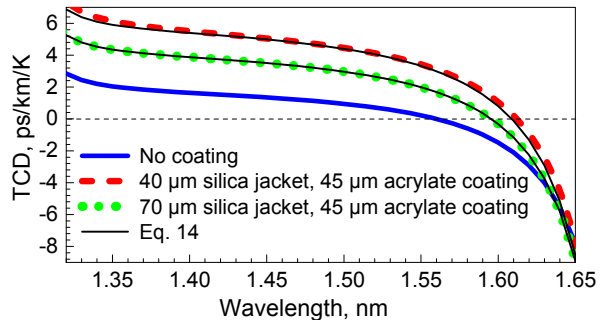

Fig. 5. Effect of polymer coating on the thermal coefficient of delay: 7-cell uncoated HC-PBGF with air filling fraction of 0.975 (for reference, solid blue); Finite-element full simulation results considering 45 μm acrylate coating and HC-PBGF with 40 μm (green, dot) or 70 μm (red, dash) silica jacket. Approximation using Eq. 14 (solid, black).

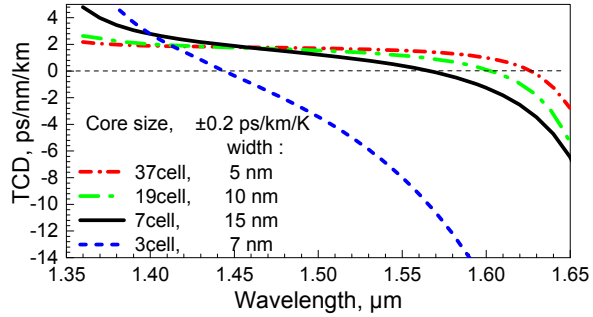

Fig. 6. Thermal coefficient of delay as function of core size: 3 (blue, dashed), 7 (black, solid), 19 (green, dash-dot), and 37-cell fibers (red, short dash-dot); the air filling fraction is kept constant at 0.975. The spectral width over which the $|TCD| \leq 0.2\ ps/km/K$ is also shown.

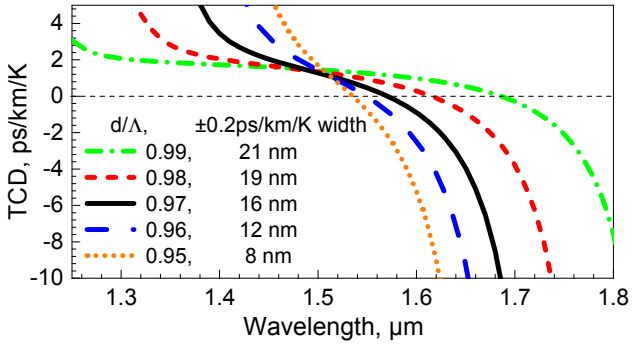

Fig. 7. Thermal coefficient of delay in 7-cell HC-PBGFs with different air-filling fraction d/Λ values: 0.95 (orange, dot), 0.96 (blue, long dash), 0.97 (solid, black), 0.98 (red, short dash), and 0.99 (green, dot dash). $|TCD| \leq 0.2\ ps/km/K$ spectral width is also shown. The cladding pitch for each fiber was scaled so as to obtain a photonic bandgap centered at $1.55 \mu m$.

A similar trend as with the core sizes we have just discussed can be expected for fibers with different cladding air-filling fractions. It is well known [24] that the higher the air-filling fraction (d/Λ), the wider the photonic bandgap and the smaller the fraction of power carried in the glass [25]. One therefore expects that in fibers with high air filling fraction, the elongation term will be the dominant contribution. This is confirmed by the simulation results shown in Fig. 7, where calculations of the $TCD(\lambda)$ (Eq. 13) as a function of the cladding's air-filling fraction has been plotted for 7-cell fibers. Although a higher air filling fraction shifts the $TDC = 0$ point towards the red edge of the bandgap, the $|TCD| \leq 0.2\ ps/km/K$ bandwidth actually gets wider (numbers shown in Fig. 7). Thus, larger air filling fractions are preferred for low thermal delay sensitivity.

From the fiber fabrication and experimental points of view, it is important to get a robust fiber design in which small variations of the

fiber cross-section (e.g., along the fiber length) or fiber bending do not alter the key properties, i.e., zero TCD wavelength and $|TCD| \leq 0.2\ ps/km/K$ bandwidth. For the 7-cell fiber design used in our experiments, we calculated that 1% change in the fiber core diameter (which we believe is the level at which the core diameter can be controlled) causes zero-TCD wavelength shift of about 1 nm with negligible contribution to $|TCD| \leq 0.2\ ps/km/K$ bandwidth. Further, we calculated that coiling this fiber with 5-cm diameter causes negligible change to the TCD characteristics.

In our analysis, we considered only the fundamental mode, although HC-PBGFs generally support several guided modes. This approach is justifiable, as HC-PGBF can be operated as effectively single-mode by optimizing the launch condition, suppressing higher order modes by more than 30 dB [25].

4. EXPERIMENT

A. Choice of fiber and its parameters

The previous section gives us guidance as to which fiber parameters to choose. Our analysis shows that 7 or 19-cell fibers are the best candidates. For the experimental proof-of-principle, we decided to use a 7-cell fiber with an air filling fraction of $d/\Lambda \approx 0.965$, which we had readily available to us. The fiber core diameter was 13.6 μm and the fundamental mode's simulated $1/e^2$ mode-field diameter was 9.7μm. Although we could not measure the attenuation precisely (due to short available length), such fibers were reported to get loss below 10 dB/km [26]. For our fiber parameters, $TDC = 0$ is expected to occur within the central part of the photonic bandgap, allowing for a straightforward observation. As we have shown earlier, the acrylate coating shifts the $TDC = 0$ to longer wavelength, which again favors (for a proof-of-principle experiment) the 7-cell fiber, as its $TDC = 0$ is further away (as compared to the 19-cell) from the long-wavelength bandgap edge.

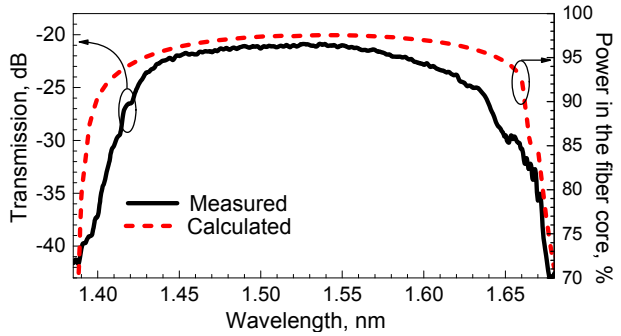

Fig. 8 Transmission characteristics of the 7-cell HC-PBGF used. Theoretical curve (red, dashed) shows the fraction of the guided mode power carried in the core. This calculation was performed using data from a scanning electron micrograph of the fiber cross-section as described in [27]. The measured transmission is shown in solid black.

As concerns the theoretically-predicted red-shift of the $TDC = 0$ point towards the bandgap edge due to the acrylate protective fiber jacket, we expected it to be very small, as the acrylate coating used (DeSolite®3471-3-14) has a very small Young's modulus of 15 MPa. This value is significantly lower than that used in [21], and in our simulations discussed above.

The measured and simulated transmission characteristics of the fiber used are shown in Fig. 8. The fiber (scanning electron micrographs of the microstructure, as well as optical microscope image are shown in Fig. 9a) had the following diameters: core: *12 μm*; microstructure: *60 μm*, silica jacket: *216 μm*; acrylate coating: *542 μm*.

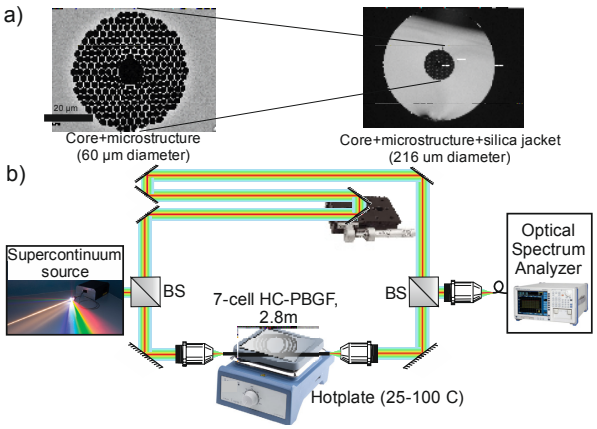

Fig. 9. (a) Micrographs of the manufactured fiber. (b) The experimental set-up. A 2.8m long sample under test is placed on a hot plate (between two metallic sheets) and connected within a balanced interferometer. The spectral phase is recorded for various fiber temperatures. BS: Beam splitter.

B. TCD characterization

We used a 2.8 m long fiber sample. The experimental set-up is shown in Fig. 9b. The fiber was coiled with a 10 cm bend diameter and placed along with a thermometer (resolution of 0.1 ^{0}C) between two metallic plates. This assembly was then put onto a hot plate that had closed-loop temperature control. To measure the $TCD(\lambda)$, we put the fiber under test into one arm of a free-space balanced Mach-Zehnder interferometer. The interference pattern (interferogram) was recorded using an optical spectrum analyzer (OSA). By locating positions of constructive and destructive interference, we extracted the spectral phase (an example is shown in Fig. 10, where each point corresponds to constructive or destructive interference). The delay through the fiber was calculated as the first derivative of the spectral phase. This is shown in Fig. 11. For better visualization of the delay at different temperatures, we show the measured delay for the lowest temperature (29^{0}C) in Fig. 11a and the difference with respect to that in Fig. 11b for another three temperatures of 47, 65, and 82^{0}C. In this figure we can appreciate that in the shorter wavelength spectral portion of the bandgap, the propagation delay through the fiber increases with the temperature. At the longer wavelength spectral region of the bandgap, we see the opposite trend. This is exactly in line with our predictions. At the wavelength of 1531 nm, the delay is insensitive to any change in temperature, which is our point of interest at which the $TCD = 0$.

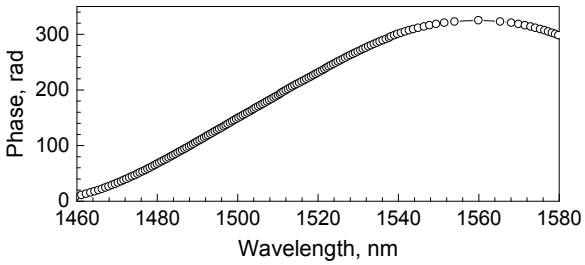

Fig. 10. Spectral phase (normalized to 1 m of fiber length) measured at 29^{0}C. Each point corresponds to one interference maxima or minima in the measured spectrogram.

The comparison between the measured result and the simulated prediction from Eq. 13 is shown in Fig. 12, where the $TCD(\lambda)$ across the bandgap is shown. To derive the experimental result, we used the data obtained at all four temperatures. Expermentally, we obtained $TCD = 0$ at *1531 nm* and with a $|TCD| \leq 0.2\ ps/km/K$ bandwidth of *11 nm*. Although there is a small discrepancy in the slope of the predicted and measured result, both curves cross the zero near the

same wavelength. The discrepancy in the slope may be attributed to the small structural differences of the real fiber versus the one modelled, which are also seen from the transmission characteirstics shown in Fig. 8.

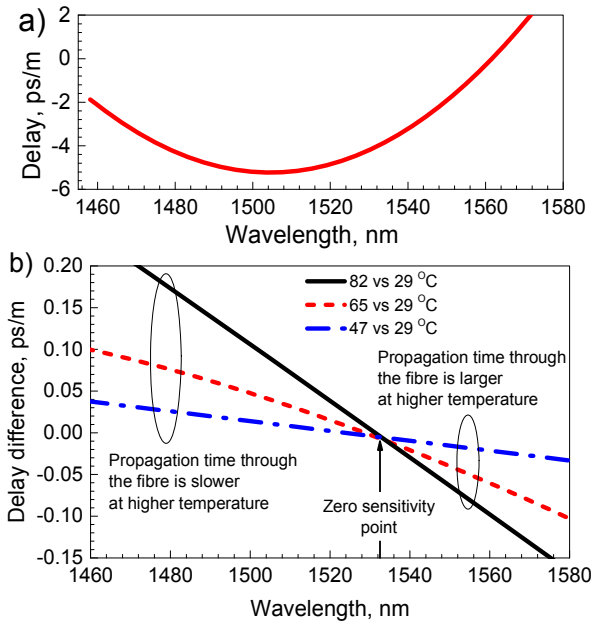

Fig. 11. Normalized propagation delay evaluated from phase responses measured at 29^{0}C (a) and its change as the fiber sample was heated to 47^{0}C, 65^{0}C, and 82^{0}C (b).

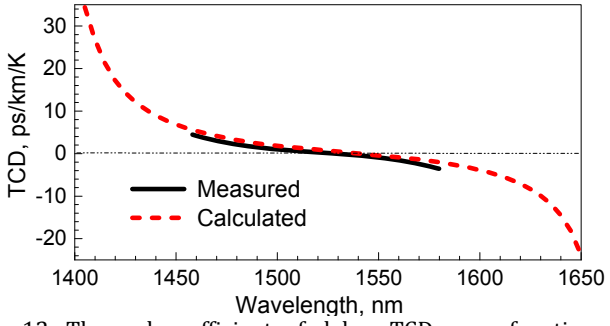

Fig. 12. Thermal coefficient of delay, TCD, as a function of wavelength: theoretical (including the acrylate jacket, Eq. 14) and experimental results.

Figure 13 shows the dispersion across the bandgap. The predicted characteristics were obtained from simulations, while the experimental data was obtained as the derivative of the propagation delay. Although there is a slight discrepancy in the calculated/predicted slope of the dispersion, the experimentally-obtained value of dispersion for $TCD = 0$ of 83 ps/km/K is very close to the predicted (in section 2A) value of 79 ps/km/K.

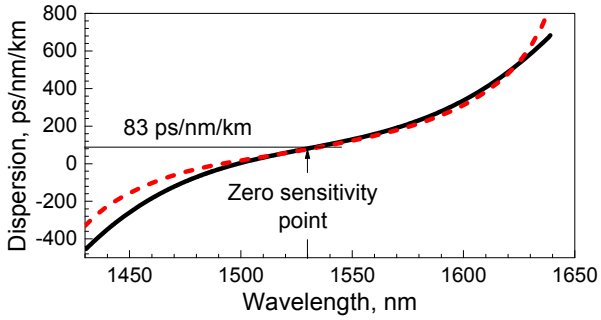

Fig. 13. Dispersion evaluated from delay (experimental data shown in Fig. 12). The experimental values are solid black; calculated values are dashed red.

6. CONCLUSIONS

We proposed, designed, and demonstrated an optical fiber in which the propagation time is fully insensitive to temperature variations ($TCD = 0$). Firstly, we used a Hollow-Core Photonic Bandgap Fiber that has inherently low *TCD*, mainly limited by the thermally-induced fiber elongation. Subsequently, we suggested compensation for the fiber elongation by making light guided in the thermally elongated fiber propagate faster.

We derived useful expressions providing us with detailed insight into the thermal behavior of HC-PBGF and into our compensation method. We also derived expressions allowing for accurate analysis of these effects in HC-PBGF, including the realistic case of fibers with a polymer protective jacket, allowing for a detailed analysis without the need to perform many time-consuming finite element simulations.

As far as straightforward physical insight is concerned, we have derived a 'zero-order approximation' expression that predicts the photonic bandgap of a bare fiber (no acrylate coating used) to red-shift with temperature at a rate of *23 pm/K* when the central operating wavelength is 1.55 μm. We also showed that this value depends solely on the thermal properties of silica and is independent of the fiber's geometry. Using this property, we found that to a zeroth-order approximation, the *TCD* depends solely on the fiber chromatic dispersion, requiring a value of 79 $ps/nm \cdot km$ to obtain $TCD = 0$. This value can be achieved for a specific wavelength in any HC-PBGF as the dispersion typically varies from a very large but negative to very large but positive value across the bandgap. However, for a practical solution, two further parameters must be optimized via the fiber design. Firstly, it is highly desirable for the dispersion of 79 $ps/nm \cdot km$ (and thus $TCD = 0$) to be achieved at wavelengths where the transmission loss is as low as possible. Additionally, to obtain low value of *TCD* over as wide a bandwidth as possible, the dispersion slope should be minimized (to keep the dispersion close to 79 $ps/nm \cdot km$ over as broad a bandwidth as possible). Experimentally, we found $TCD = 0$ occurred at chromatic dispersion of 83 $ps/nm \cdot km$. This value is very close to the here-in predicted value of 79 $ps/nm \cdot km$, verifying experimentally the above claims/numbers derived.

The fiber microstructure cross section changes due to three effects. We found numerically that the transverse expansion and photo-elastic effects produce relatively small changes in the guided mode propagation speed and almost cancel each other out. Thus, the dominant effect used for compensation of the temperature-induced fiber elongation is the thermo-optic effect (change of the refractive index with temperature).

We also studied theoretically the effect of a protective polymer jacket typically made from an acrylate. The coating (e.g. of Desolite3-14) increases the rate at which the fiber elongates with increased temperature. The jacket also introduces changes in the fiber cross-section. We found that the most significant change to the fiber cross-section is the change in the core radius, which allowed us to derive a simple expression to quantify the jacket influence on *TCD*. Through numerical analysis, we showed how the thickness of the glass that surrounds the microstructure (glass jacket) and the thickness of the protective coating both influence the performance, generally shifting the $TCD = 0$ point towards longer wavelengths. It is worth mentioning that the glass jacket thickness has no influence on the TCD when no protective coating is applied to the fiber.

Once we had gained a deep understanding of the effects involved we evaluated the performance of practical fiber designs: more specifically those that are manufactured today that have 3,7,19, or 37-cell cores and an air filling fraction of 0.90-0.99. Both these parameters influence the fiber chromatic dispersion and its slope, which are the key parameters for our compensation method as described above. We found that fibers with 7 or 19-cell cores and an air filling fraction >95% are likely to give an optimum compromise between the low-thermal

sensitivity bandwidth (here defined as $|TCD| \leq 0.2\ ps/km/K$) being up to *10-20 nm*, and insertion loss (by shifting the $TCD = 0$ wavelength well away from the bandgap edge).

To confirm our method experimentally, we used a 7-cell HC-PBGF with an air-filling fraction of 0.965, which operated in the 1550-nm spectral region. Using balanced spectral interferometry, we measured the *TCD* across the bandgap at four temperature settings, spanning 29 to 82^{0}C. The results are in excellent agreement with theoretical predictions, confirming the accuracy of our simulations. Most importantly, we observed for the first time, to the best of our knowledge, $TDC = 0$ in an optical fiber. We obtained it at a wavelength of *1531 nm* with an 11 *nm* bandwidth over which the $|TCD| \leq 0.2\ ps/km/K$, corresponding to a 90% compensation of the fiber elongation. Our simulations suggest that $|TCD| \leq 0.2\ ps/km/K$ over twice as large a bandwidth (in excess of *20 nm*) could be straightforwardly achieved with an optimized fiber design (e.g., using air-filling fractions of >99%).

Our result represents the first demonstration of $TCD = 0$ in a silica fiber without the use of any (exotic) compensating coating. This fiber is 10 times less temperature-sensitive than previously-demonstrated HC-PBGF and is almost 200 times less sensitive than standard solid-core fiber over a bandwidth as large as 11 nm. Over a smaller bandwidth (e.g., 2 nm) our demonstration shows an unprecedented 1000 times lower thermal sensitivity as compared to solid core fiber.

The extremely low levels of thermal sensitivity of propagation delay through an optical fiber demonstrated here should bring significant improvements in the generation and transfer of signals with precise frequency and timing, allowing the levels of stability only now achievable in specialized metrology laboratories to be realized in the external world. We expect that the ability to provide stable latency will allow new approaches in well-established fields, e.g., enable time-synchronous data transfer in optical communications, allowing, e.g., for lower latency and simplification of data processing., and help open up emerging new fields such as relativistic geodesy.

Funding. Engineering and Physical Sciences Research Council (EPSRC) (EP/K003038/1, Fellowship; EP/I061196X EP/I01196X/1, Photonics Hyperhighway). Royal Society and Wolfson foundation.

Acknowledgment. The data for this work is accessible through the University of Southampton Institutional Research Repository (doi: XXXXX).

REFERENCES

1. F. Loehl et al., "Measurement an stabilization of the bunch arrival time at FLASH," Proceedings of the 11th European Particle Accelerator Conference (EPAC'08), paper THCP158, pp. 3360-3362, Genoa, Italy, 2008.
2. G. Grosche, O. Terra, K. Predehl, R. Holzwarth, B. Lipphardt, F. Vogt, U. Sterr, and H. Schnatz, "Optical frequency transfer via 146 km fiber link with 10^{-19} relative accuracy," Opt. Lett. 34, 2270 (2009).
3. M. Koivisto et al, "Joint Device Positioning and Clock Synchronization in 5G Ultra-Dense Networks," arXiv: 1604.03322v1 (2016).
4. C. Lisdat et al, "A clock network for geodesy and fundamental science, Nature Comm. 7, 12443 (2016).
5. J. Flury, "Relativistic geodesy," J. of Physics: Conference Series 724, 012051 (2016).
6. F. Kéfélian, H. Jiang, P. Lemonde, and G. Santarelli, "Ultralow-freqeuncy-noise stabilization of a laser by locking to an optical fiber-delay line," Opt. Lett. 7, 914 (2009).
7. X.S. Yao and L. Maleki, "Optoelectronic microwave Oscillator," J. Opt. Soc. Am. B 13, 1725 (1996).
8. G.A. Cranch and G.A. Miller, "Fundamental frequency noise properties of extended cavity erbium fiber lasers," Opt. Lett. 36, 906 (2011).
9. M. Bousonville et al, "New phase stable optical fiber,"Proc. of Beam Instrumentation Workshop (BIW 2012), paper MOPG033, 101, Newport News, VA, USA, April 15-19, 2012.
10. R. Slavík, G. Marra, E. Numkam Kokoua, N. Baddela, N.V. Wheeler, M. Petrovich, F. Poletti, and D.J. Richardson, "Ultralow thermal sensitivity of phase and propagation delay in hollow core optical fibres, " Sci. Rep. 5, 15447 (2015).
11. J.D. Shephard, J.D.C. Jones, D.P. Hand, G. Bouwmans, J.C. Knight, P.J. Russel, and B.J. Mangan, "High energy nanosecond laser pulses delivered single-mode through hollow-core PBG fibers," Opt. Express 12, 717 (2004).
12. F. Poletti, N.V. Wheeler, M.N. Petrovich, N. Baddela, E. Numkam-Fokuoa, J.R. Hayes, D.R. Gray, Z. Li, R. Slavík, and D.J. Richardson, "Towards high-capacity fibre-optic communications at the speed of light in vacuum," Nat. Photonics 7, 279 (2013).
13. L. Olanterä, C. Sigaud, J. Troska, F. Vasey, M.N. Petrovich, F. Poletti, N.V. Wheeler, J.P. Wooler, and D.J. Richardson, "Gamma irradiation of minimal latency Hollow-Core Photonic Bandgap Fibres," J. of Instrumentation 8, C12010 (2013).
14. T. A. Birks, D. M. Bird, T. D. Hedley, J. M. Pottage, and P. St.J. Russell, "Scaling laws and vector effects in bandgap-guiding fibres," Opt. Express 12, 69 (2004).
15. J.D. Joannopoulos, S.G. Johnson, J.N. Winn, and R.D. Meade, Photonic Crystals: Molding the Flow of Light, 2nd Edition, Princeton University Press (2008) p. 20.
16. American Institute of Physics Handbook (McGraw-Hill, New York), 1957.
17. K. Saitoh and M. Koshiba, "Leakage loss and group velocity dispersion in air-core photonic bandgap fibers," Opt. Express 11, 3100-3109 (2003).
18. M. Skorobogatiy et al, "Analysis of general geometric scaling perturbations in a transmitting waveguide: fundamental connection between polarization-mode dispersion and group-velocity dispersion," J. Opt. Soc. Am. B 19, 2867 (2002).
19. N. C. Frateschi and A.R.B. De Castro, "Perturbation Theory for the Wave Equation and the "Effective Refractive Index" Approach," IEEE J. Quantum Electron. Qe-22, 12 (1986).
20. K. Zhang and D. Li, Electromagnetic Theory for Microwaves and Optoelectronics, 2nd Edition, Springer (2008) p. 313.
21. V. Dangui, H.K. Kim, M.J.F. Digonnet, and G.S. Kino, "Phase sensitivity of temperature of the fundamental mode in air-guiding photonic-bandgap fibers," Opt. Express 13, 6669 (2005).
22. M. Skorobogatiy, S.A. Jacobs, S.G. Johnson, and Y. Fink, "Geometric variations in high index-contrast waveguides, coupled mode theory in curvilinear coordinates," Opt. Express 10, 1227 (2002).
23. M.N. Petrovich, F. Poletti, A. van Brakel, and D.J. Richardson, "Robustly single mode hollow core photonic bandgap fiber, Opt. Express 16, 4337 (2008).
24. N.A. Mortensen and M.D. Nielsen, "Modeling of realistic cladding structures for air-core photonic bandgap fibers," Opt. Lett. 29, 349 (2004).
25. F. Poletti, "Hollow core fiber with an octave spanning bandgap," Opt. Lett., 35, 2837 (2010).
26. R. Amezcua-Correa, F. Gerome, S.G. Leon-Saval, N.G.R. Broderick, T.A. Birks, and J.C. Knight, "Control of Surface modes in low loss hollow-core photonic bandgap fibers," Opt. Express 16, 1142-149 (2008).
27. E.R. Numkam Fokoua, S.R. Sandoghchi, Y. Chen, G.T. Jasion, N.V. Wheeler, N.K. Baddela, J.R. Hayes, M.N. Petrovich, D.J. Richardson, and F. Poletti, "Accurate modelling of fabricated hollow-core photonic bandgap fibers," Opt. Express 23, 23117-23132 (2015).
28. J.C. Owens, "Optical Refractive Index of Air: Dependence on Pressure, Temperature and Composition," Appl. Opt. 6, 51-59 (1967).

Appendix 1: Refractive index of air

According to [28], the refractive index of air as a function of temperature and pressure is given by:

$$\frac{n^2-1}{n^2+2}=\sum\frac{n_{0i}^2-1}{n_{0i}^2+2}\frac{\rho_i}{\rho_{0i}} \tag{14}$$

where i extends over the individual components of the air (e.g., dry CO_2 -free air, water vapour and CO_2), n_{0i} and ρ_{0i} are the refractive index and density of the i-th component at standard temperature and pressure conditions and ρ_i the density of the i-th component at the given pressure and temperature conditions. The formulas for the refractive indices of these components can be found in [28]. Assuming that the air holes in our HC-PBGFs are filled with dry air and 3% CO_2 and that this mixture behaves as an ideal gas, we found that when both ends of the fibers are spliced and therefore the amount of air within the fiber kept constant, the refractive index of air changes at an approximate rate of $-3\times10^{-9}/K$. Using this value in Eq. 11 and 13, we find that the contribution of the air refractive index to the TCD is no more than $10^{-2}ps/km/K$. This justifies neglecting this effect in our analysis.